POAC'25
St. John's, Newfoundland and Labrador, Canada

Proceedings of the 28th International Conference on Port and Ocean Engineering under Arctic Conditions
Jul 13-17, 2025
St. John's, Newfoundland and Labrador
Canada

High-Resolution Simulation of Sea Ice Dynamics Using a Nested Modeling Approach

Jiaming Chen[1], Wenjun Lu[2], Runxin Xu[3], Shifeng Ding[4], Li Zhou[3,*]
[1] School of Naval Architecture and Ocean, Engineering, Jiangsu University of Science and Technology, Zhenjiang 212100, China
[2] Department of Civil and Transport Engineering, Norwegian University of Science and Technology, 7491 Trondheim, Norway
[3] State Key Laboratory of Ocean Engineering, Shanghai Jiao Tong University, Shanghai, China
[4] School of Naval Architecture, Ocean & Civil Engineering, Shanghai Jiao Tong University, Shanghai, China

ABSTRACT

The dynamics of sea ice play a crucial role in climate research and polar vessel navigation, particularly in capturing the behavior of small-scale features such as ice floes and fractures. However, traditional continuum models based on the Viscous-Plastic (VP) theory struggle to accurately reproduce these features at high resolution, while Discrete Element Models (DEM), although suitable for small-scale modeling, are limited in their application to large-scale sea ice simulations due to computational constraints. This study employs a nested modeling approach, embedding DEM within a continuum model to simulate small-scale ice floe dynamics. A real-time ice field model was constructed using high-resolution satellite imagery, and large-scale sea ice drift velocities provided by the continuum model were applied as boundary conditions to simulate ice drift and deformation. The results demonstrate that the nested model can capture regions of concentrated sea ice deformation in areas with high ice density, showing strong agreement with satellite observations. The model successfully simulated ice drift and deformation parameters across different temporal scales, highlighting significant spatial distributions of local deformation. Additionally, ice deformation exhibited high sensitivity to tidal forcing, with tidal effects having a pronounced impact on ice dynamics at shorter timescales. The nested model offers a novel approach for predicting sea ice behavior at high resolution, presenting potential applications in polar vessel navigation planning and climate research.

KEY WORDS: Sea Ice; Ice Dynamics; Discrete element method; Nested Model; Ice drift.

INTRODUCTION

With the ongoing effects of global warming, the extent and thickness of Arctic Sea ice are

decreasing, presenting new opportunities for polar exploration and the development of Arctic shipping routes. In this context, research on sea ice drift holds dual strategic significance. The construction of high-precision ice motion models enables real-time ice forecasting, optimal route planning, and ship icebreaking capability assessments for the Northwest and Northeast Passages, thereby enhancing both the economic efficiency and safety of Arctic navigation. The sea ice dynamics model incorporating multi-physical field coupling facilitates the analysis of energy transfer mechanisms at the ice-water-atmosphere interface, enabling the prediction of ice ridge evolution under the influence of sea ice drift. This, in turn, provides a scientific basis for the ice-resistant design of critical infrastructure, such as oil and gas platforms in the Arctic region. With advancements in satellite remote sensing and numerical simulations, the study of sea ice drift has transitioned from mere phenomenological descriptions to multi-scale coupling mechanism analyses. Therefore, investigating the motion response and deformation behavior of sea ice under the combined effects of wind, waves, and currents is of substantial academic and practical importance.

The sea ice undergoes continuous drift and deformation under the combined effects of wind stress, ocean current stress, Coriolis force, internal ice stress, and waves. (Yu et al., 2019) conducted Bohai Sea ice drift experiments using a simulated ice model and found that both tidal currents and wind play significant roles in sea ice drift, with tidal currents being the dominant factor. When the wind direction aligns with the current direction, ice movement is facilitated, whereas when the two are opposite, ice movement is inhibited. The influence of tidal currents on sea ice drift exhibits periodicity, while long-distance sea ice drift is primarily driven by the unidirectional force of the wind (Liu and Wu, 2017). (Zhang et al., 2023) established an ice-ocean coupled mathematical model to investigate the movement patterns of high-risk ice particles near water intakes under cold wave conditions, revealing that ice particles are unlikely to enter the intake. (Yuan et al., 2021) find that remote sensing data can be used to monitor sea ice motion, providing key movement parameters such as ice velocity, displacement, and trajectory. (Song et al., 2018) developed a GPS-based sea ice positioning and tracking system capable of accurately mapping ice trajectories. While physical experiments using sea ice models and mathematical models based on the Lagrangian method can intuitively present localized sea ice drift, they fail to capture the overall movement patterns of Bohai Sea ice. Although remote sensing imagery can depict the spatial distribution of sea ice across the entire Bohai Sea, it is constrained by observation time and conditions, making it difficult to provide continuous and comprehensive spatiotemporal data. Additionally, remote sensing observations only reflect sea ice drift as a result of the combined action of multiple dynamic factors, without the ability to isolate the effects of individual factors. In contrast, numerical simulations offer significant advantages in analyzing the physical properties and evolution of sea ice, allowing for a focused examination of specific influencing factors. This provides crucial insights for predicting sea ice trends, supporting ice zone navigation, and facilitating resource utilization. (Tsarau et al., 2024a) and (Tsarau et al., 2024b) used continuum model nested DEM model to study sea ice drift and overall deformation at large scales.

Thus, the large-scale coverage of the continuum model can be effectively integrated with the high local resolution of the discrete element method (DEM). Building upon this concept, we have conducted a feasibility study on regional sea ice modeling that incorporates a nested non-smooth DEM within a continuum framework. Embedding an efficient DEM into a regional sea ice model holds significant potential, particularly for applications such as optimizing shipping routes and facilitating commercial operations in the marginal ice zone (MIZ). Additionally, this model can offer valuable insights into the dynamics of drift and

deformation within specific sea ice, enhancing our understanding of its mechanical behavior and evolution.

NUMERICAL APPROACH

YOLOv8 model

YOLOv8 offers fast detection speeds and can meet the real-time requirements of ships navigating in polar regions (Wang et al., 2024). It employs an enhanced Cross-Stage Partial Darknet as its backbone network, leveraging the Cross-Stage Partial Network (CSPNet) to improve feature representation. In the neck, YOLOv8 utilizes the Path Aggregation Network (PANet) for feature fusion, aggregating features from different scales to enhance detection performance. The output layer of YOLOv8 consists of multiple scale-specific prediction heads, with each head responsible for detecting objects of different sizes. This architecture enables YOLOv8 to perform efficient and accurate real-time object detection. An overview of YOLOv8 is shown in Figure 1. By inputting sea ice images into a trained YOLOv8 model, individual sea ice floes can be detected. The model used in this study was fully pre-trained and fine-tuned in previous research.

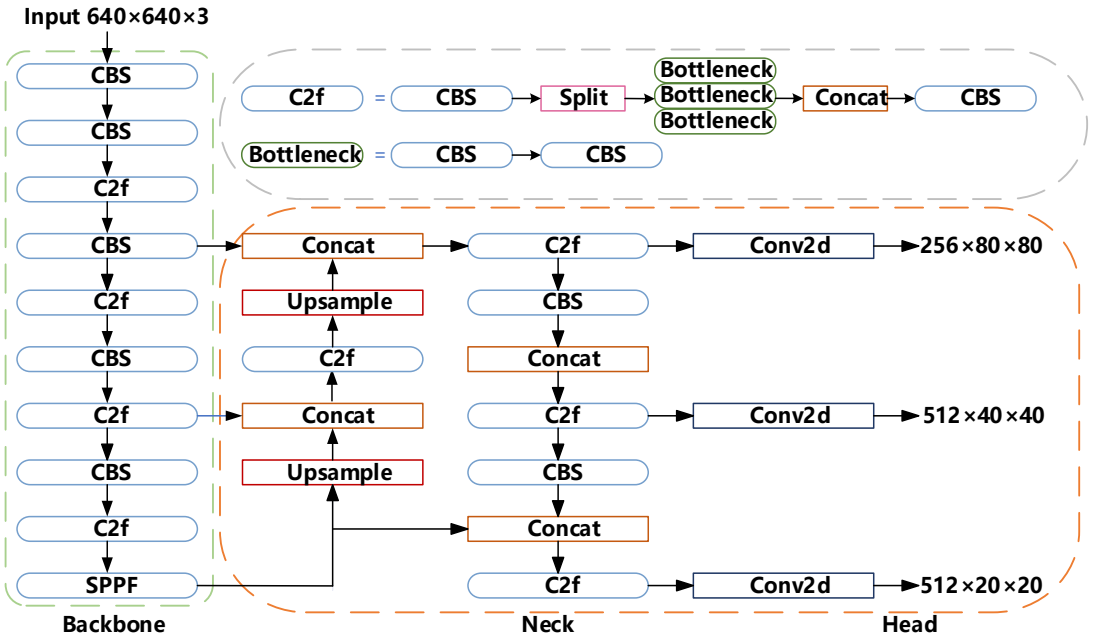

Figure 1. YOLOv8 Network structure

During the training process of YOLOv8, a series of key hyperparameters were set to ensure the model could effectively learn sea ice features and achieve optimal performance in detection tasks. The number of classes was set to 1, enabling the model to focus solely on identifying sea ice targets, thereby avoiding interference from multiple classes and improving classification accuracy. The number of training epochs was set to 500 to provide sufficient learning time, allowing the model to extract deeper features and enhance generalization ability.

A relatively high learning rate of 0.01 was selected to accelerate convergence, although it requires careful tuning in combination with other hyperparameters to avoid instability during training. Considering the limitations of computational resources, the batch size was set to 2, which reduces GPU memory consumption and maintains training stability.

To further optimize gradient updates, the momentum was set to 0.8, making the training process smoother, reducing oscillations, and improving convergence efficiency. Additionally, to prevent overfitting, weight decay was introduced with a value of 0.0005. This L2 regularization term constrains model complexity and improves generalization capability. All training parameters of YOLOv8 can be seen in Table 1.

Table 1. Training parameters of YOLOv8

Parameters	Value	Parameters	Value
num_class	1	batch_size	2
epoch	500	momentum	0.8
learning_rate	0.01	weight_decay	0.0005

Sea-ice dynamics in a continuum framework

Continuum models for sea ice dynamics describe the motion of ice mass per unit area (m) by solving the momentum equation within a fixed Eulerian mesh, accounting for the effects of winds and ocean currents. One example is CICE, the Los Alamos Sea Ice Model, which is integrated into several Earth System Models (CICE Consortium, 2021). This model employs a two-dimensional momentum equation obtained by vertically integrating the three-dimensional equation over the ice thickness (Hunke and Dukowicz, 1997).

$$m\frac{\partial \mathbf{u}}{\partial t} = \nabla \cdot \sigma + \boldsymbol{\tau}_a + \boldsymbol{\tau}_w - \hat{\boldsymbol{k}} \times mf\mathbf{u} - mg\nabla H_{\mathrm{o}} \tag{1}$$

Where $\mathbf{u}$ represents the ice velocity, σ denotes the internal stress tensor, the terms $\boldsymbol{\tau}_a$ and $\boldsymbol{\tau}_w$ correspond to wind and ocean stresses, respectively. The final two terms on the right-hand side account for stresses arising from Coriolis effects and the sea surface slope. The ocean stress, acting tangentially to the ice, is expressed as follows.

$$\boldsymbol{\tau}_w = C_w \rho_w |\, \boldsymbol{U}_w - \mathbf{u}| \left[(\boldsymbol{U}_w - \mathbf{u}) \cos\theta + \hat{\boldsymbol{k}} \times (\boldsymbol{U}_w - \mathbf{u}) \sin\theta \right] \tag{2}$$

Here ρ_w, C_w and $\boldsymbol{U}_w$ represent the water density, drag coefficient, and current velocity, respectively. The vertical unit vector is denoted as $\hat{\boldsymbol{k}}$, and θ is the turning angle between geostrophic and surface currents. This turning angle is necessary when the upper layers of the ocean model cannot fully resolve the Ekman spiral within the boundary layer. If the top layer is sufficiently thin relative to the typical depth of the Ekman spiral, assuming θ=0 provides a reasonable approximation. Following the approach in (CICE Consortium, 2021), we assume the top layer is thin enough for this approximation to hold. Similarly, wind stress can be expressed in terms of surface wind velocity.

$$\boldsymbol{\tau}_a = C_a \rho_a |\, \boldsymbol{U}_a |\, \boldsymbol{U}_a \tag{3}$$

where ρ_a and C_a represent the air density and drag coefficient, respectively; while $\boldsymbol{U}_a$ denotes the wind velocity measured at 10 m. CICE discretizes the momentum equation in time and then solves it using methods such as the elastic-viscous-plastic (EVP) ice dynamics scheme (Hunke et al., 2020). In this approach, σ_{ij} is determined based on a regularized form of the viscous-plastic (VP) constitutive law, which models the ice pack as a visco-plastic material that exhibiting plastic flow under typical stress conditions but behaving as a linearly viscous

fluid when strain rates are low. At each integration time step, typically around one hour, CICE computes the velocity **u** and generates various outputs, including ice drift direction, velocity, concentration, and thickness. These parameters can be used as initial and boundary conditions for a nested discrete element method (DEM) model.

Discrete element model

The DEM model used in this study solves the 3D rigid-body equations of motion, incorporating the same force components as those on the right-hand side of Eq. (1). However, since the ice field is now represented as discrete floes, contact forces between these rigid bodies must be modeled in place of the internal stress tensor from Eq. (1), and fluid forces need to be integrated over their surfaces. Additionally, the force term related to the sea surface slope is omitted, as its influence is generally negligible compared to the dominant forces at play (Leppäranta, 2011).

A non-smooth DEM approach, formulated at the level of velocities and impulses rather than the conventional acceleration and force-based models, was employed. This method offers a distinct advantage in efficiently resolving numerous contact interactions between floes, including Coulomb friction and ice crushing (van den Berg et al., 2018). The model incorporates various analytical solutions for ice fracture resulting from interactions with icebreaking vessels, enabling validation against field measurements of icebreaker performance and ice management operations data (Lubbad et al., 2018). However, these fracture solutions cannot be directly applied to large-scale sea ice modeling, as they were specifically developed for ice-structure interactions occurring over ship-length scales and may not hold at broader scales.

Although the current model does not fully capture the physics of ice fracture, it can be parameterized to estimate local deformations within an ice field due to processes such as floe crushing and rafting. The floe-floe interaction model proposed by van den Berg et al. (2018) assumes that local ice crushing takes place. In numerical simulations, this phenomenon is represented by floe overlap, with the corresponding restoring forces calculated based on precise contact geometries and the material properties of the interacting floes. The original model by van den Berg et al. (2018) assumes a constant crushing pressure (or plastic limit stress) during indentation, which is parameterized as described in Eq. (4):

$$F_{cr} = A_{proj} \cdot CSE \tag{4}$$

Where F_{cr} is the limit of contact force above which crushing occurs, A_{proj} is the contact projected area, and CSE is the crushing specific energy of sea ice. Below F_{cr}, the contact force is calculated such that the floes' relative velocity in the normal direction of their contact interface remains zero, or the force is zero in the case of separating floes.

Embedding DEM inside a larger sea-ice model

Our embedded DEM was initially designed to run in parallel with CICE, but it can be used with any alternative tool for predicting large-scale sea ice motion, as no direct coupling exists between the models. In the current setup, the DEM domain starts as a square region enclosed by four linear boundaries containing discrete ice floes. These boundaries are rigid yet capable of independent movement, governed by interpolated ice-drift velocities derived from the continuum model (or other predictive tools) at its computational mesh nodes. As the boundaries shift, they may trap the floes inside, preventing ice flux across them.

Consequently, the DEM domain deforms while drifting over the stationary continuum model mesh.

The DEM dynamics are driven by atmospheric and oceanic forcing data, which may offer higher temporal and spatial resolution than the input used in the continuum model. In typical applications, the DEM domain spans approximately 100 km, with time scales ranging from fractions of a second to several days. The resolution of input data must be sufficient to capture processes at these scales. Given the relatively short time spans considered, thermodynamic processes are not included within the DEM domain.

CICE operates with a typical time step of 1 hour, whereas the DEM solves sea ice dynamics at 0.2-second intervals. The larger of these two time steps serves as the communication interval, during which CICE data is used to update the boundary conditions in the DEM. Communication with the DEM is facilitated through a TCP/IP network interface, enabling data exchange between different machines over a network.

In this simulation, data is transmitted only from CICE to the DEM. Since CICE, with its larger time step, may run significantly faster than the DEM, the predicted continuum ice velocity is stored in a buffer. The DEM's TCP/IP module then retrieves this hourly data, interpolates it for application at the DEM boundaries, and subsequently updates the boundary conditions accordingly.

SIMULATION RESULTS

DEM ice fields from Satellite imagery

Based on data availability, this study focuses on sea ice located beyond the marginal ice zone but within a 100 km range. A suitable region was identified using Sentinel-2 satellite imagery, with coordinates at 76.43°N latitude and 7.81°E longitude. The image was captured on May 4, 2022, as shown in Figure 2a. It features minimal cloud cover, allowing clear identification of floating ice and island boundaries. The images cover an approximately 100*100 km geographic region and were acquired using Sentinel-2 sensors in the visible spectral bands with a spatial resolution of 10 meters. Further details regarding the Sentinel-2 mission, including sensor characteristics and collected data, can be found in Drusch (2012).

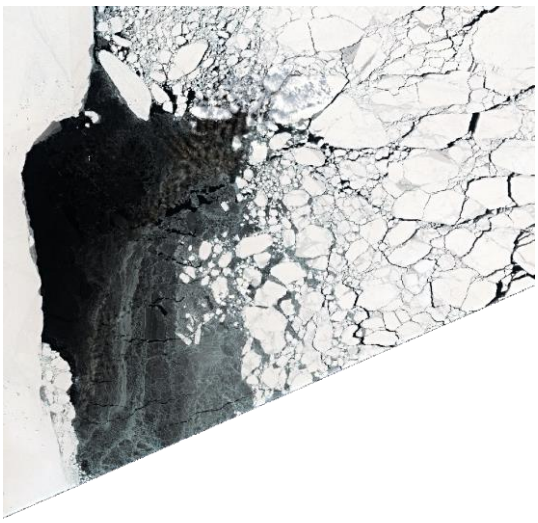

Figure 2. Sentinel-2 optical imagery of the same area Source: https://dataspace.copernicus.eu/

In this study, image processing techniques were used to provide the initial sea ice configuration for our DEM model, corresponding to the ice field shown in Figure 2a. First, at a 100 km*100 km scale, the continuum model was employed to compute sea ice drift velocity, which was then used as the boundary condition for the small-scale DEM.

The upper-left corner of the satellite image was selected as the local study area. Within this region, ice compression, deformation, and fracturing caused by sea ice drift are illustrated in Figure 3a, while Figure 3b shows the sea ice distribution in the DEM computational model.

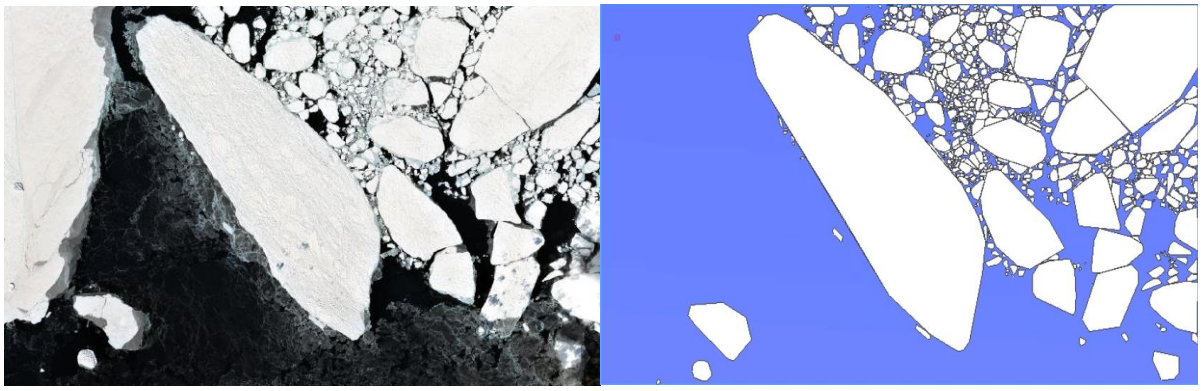

Figure 3. The local area of Sentinel-2 optical imagery and ice field in the DEM model.

Data sources

Optical satellite imagery does not provide ice thickness data, which is essential for initializing 3D floes in the DEM model. To address this, we utilized ice-thickness data from the CS2–SMOS product (Ricker et al., 2017). This dataset integrates thickness estimates from the CryoSat-2 (CS2) altimeter for ice thicker than 1 m and the Soil Moisture and Ocean Salinity (SMOS) satellite for thinner ice, offering comprehensive Arctic-wide coverage across the entire thickness range. For our study area, the weekly average ice thickness from CS2–SMOS is 1.7m.

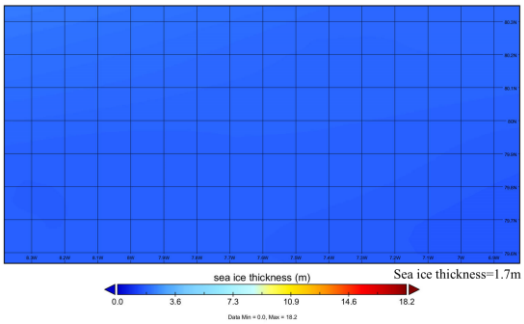

Figure 4. Sea ice thickness distribution map

After initializing the ice field in the nested model, the force terms in Eq. (1) must be specified. For wind forcing, we used 10-m wind data from the NORA3 reanalysis, a high-resolution mesoscale weather simulation covering the North Sea, Norwegian Sea, and parts of the Barents Sea. This dataset is downscaled from the advanced ERA5 reanalysis (Solbrekke et al., 2021). Our DEM model incorporated hourly wind speeds and directions at a 3-km horizontal resolution.

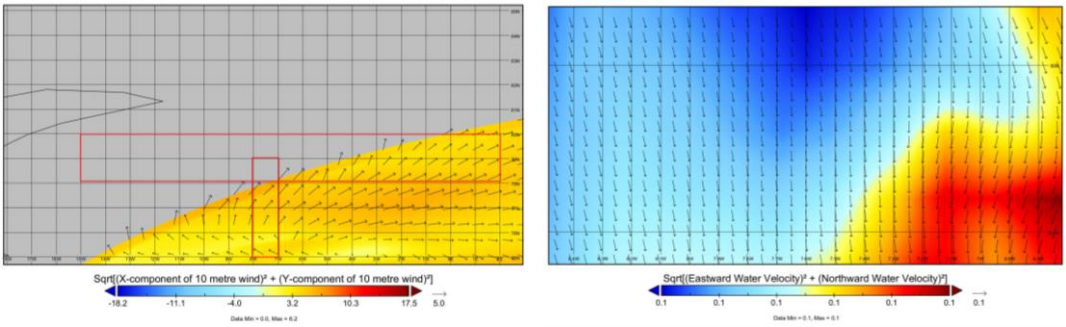

Figure 5. Scaled wind vectors (left) and total current vectors (right)

We also incorporated the Hybrid Coordinate Ocean Model (HYCOM), which offers 41-layer ocean data on a 1/12° global grid with an average resolution of 6.5 km (Chassignet et al., 2009). While HYCOM provides non-tidal surface currents at a 3-hour temporal resolution, we interpolated this data and incorporated a tidal component to generate hourly estimates for updating our DEM model. This adjustment was necessary due to the absence of 2016 hourly current data that includes both tidal and non-tidal contributions in the upper ocean layer.

The tidal component was derived using the Arctic 2 km Tide Model (Arc2kmTM) developed by Howard and Padman (2021). Arc2kmTM is a barotropic tide model with a 2x2 km polar stereographic grid, based on the Regional Ocean Modeling System (ROMS). It provides spatial grids of complex amplitude coefficients for sea surface height and depth-integrated currents for eight primary tidal constituents: four semidiurnal (M2, S2, K2, N2) and four diurnal (K1, O1, P1, Q1). By applying the model and its bathymetry data for our study area, we obtained depth-averaged tidal currents, which were then added to the HYCOM current to estimate the total surface current. The mean values of both current components, along with wind data, are summarized in Table 2.

HYCOM has been integrated with the Los Alamos Sea Ice Model (CICE) in a global prediction system operated by the U.S. Navy through the Naval Oceanographic Office. Data fields are accessible via hycom.org, with both sea-ice and ocean models running on the same 1/12° grid. This system provides nowcast/forecast and historical datasets, including sea-ice velocity, which can be utilized as boundary conditions in our nested model.

Table 2. Mean wind and current data

	1-hour mean	24-hour mean	Difference
Ice thickness/m	1.70	1.70	0%
Wind speed/ms^{-1}	3.8	4.2	10.53%
Wind direction/°	152	148	-2.63%
Total current speed/ms^{-1}	0.11	0.014	-87.27%
Total current direction/°	283	294	3.89%

Ice drift

Wind and currents are the primary driving forces acting on sea ice motion. This section aims to investigate sea ice movement under the combined influence of tidal currents and wind fields. We selected sea ice numbered #6 and #414 as specific study objects to analyze their motion under different environmental loads.

Figure 6(a) illustrates the variation of the rotational angle of sea ice #414 over time, while Figure 6(b) presents the distribution of sea ice at the end of the simulation. As shown in Figure 6(a), the rotational angle of sea ice #414 remains relatively stable in the initial stage, maintaining a range of approximately 0.55 to 0.6. Subsequently, it begins to increase slowly at a low growth rate. Later, the angle rapidly rises to a maximum value of 1.35, indicating the influence of strong external forces. Since the simulation in this study uses the average flow velocity over time, the increase in angle is likely caused by interactions between sea ice floes. After reaching the peak, the angle gradually decreases to 0.7, suggesting that the external forces weaken and the ice rotation stabilizes. Figure 6(b) displays the spatial distribution of sea ice #414 at the end of the simulation. The final position is marked in the red rectangular box with a purple area. The sea ice floe is located at the boundary of a densely packed broken-ice region, characterized by an irregular shape and surrounded by multiple smaller ice pieces, indicating that it experienced fragmentation, collisions, or compressive locking during its movement. By combining the rotational angle curve in Figure 6(a) with the final distribution in Figure 6(b), it can be inferred that the maximum rotational angle (~1.35 degree) likely corresponds to the moment when the floe experienced the strongest external force. Its final position near the fragmented ice zone suggests that its rotational motion was constrained by surrounding small ice pieces, leading to a reduction in angle and eventual stabilization.

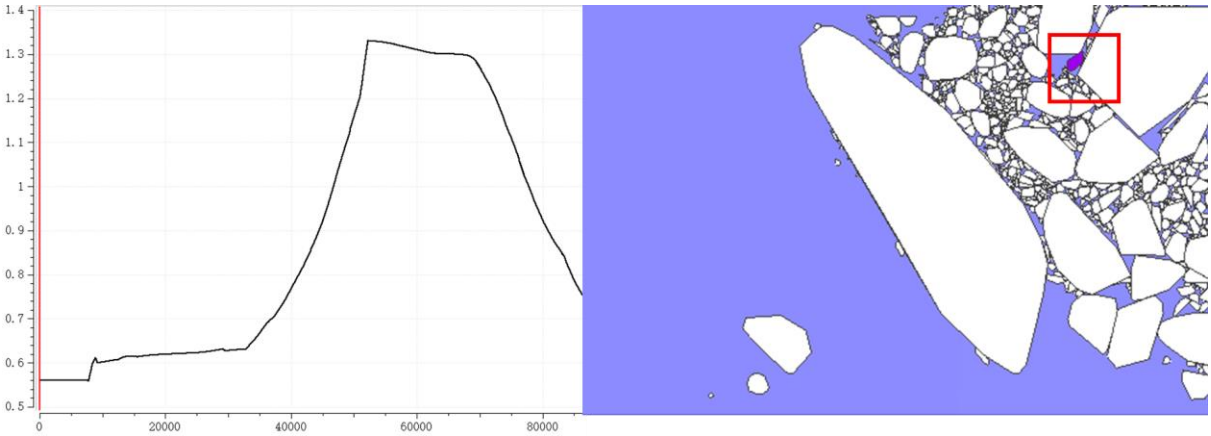

Figure 6. Sea ice rotation angle time history curve of No. 414 and sea ice distribution at the end of calculation

Figure 7 illustrates the variation of the rotational angle of sea ice #6 over time and its distribution at the end of the simulation. As shown in Figure 7(a), the rotational angle of sea ice #6 remains relatively stable in the initial stage, maintaining a value of approximately 0.63. It then gradually increases to a maximum of 0.635, with only a slight change, indicating that the external forces acting on it during this phase are weak. Subsequently, the angle gradually decreases to 0.585, suggesting that external forces cause a reduction in its rotational motion, eventually leading to stabilization. Figure 7(b) presents the spatial distribution of sea ice #6 at the end of the simulation. The final position is marked in the red rectangular box with a purple area. This sea ice is a relatively large, single ice block with an intact shape, surrounded mainly by small ice pieces and open water. This suggests that it did not experience significant fragmentation or collisions during its movement and was primarily influenced by wind and ocean currents. By combining the rotational angle curve in Figure 7a with the final distribution in Figure 7(b), it can be inferred that the maximum rotational angle (~0.635) of sea ice 6 is relatively small, indicating that its rotational motion was limited throughout the simulation. Additionally, its final position is relatively isolated, showing no significant influence from the fragmented ice zone.

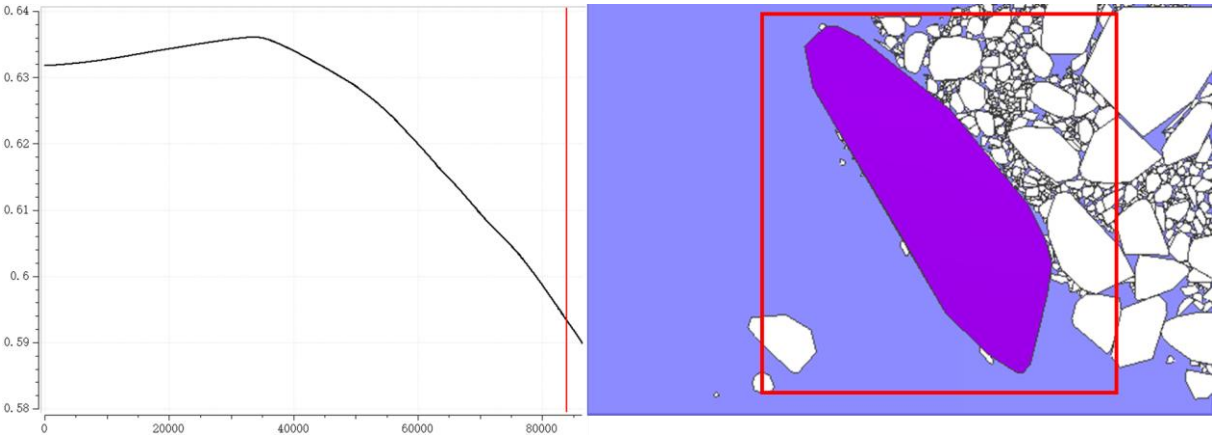

Figure 7. Sea ice rotation angle time history curve of No. 414 and sea ice distribution at the end of calculation

CONCLUSIONS

This study employs a nested modeling approach to conduct high-resolution numerical simulations of sea ice dynamics and provides a detailed analysis of sea ice motion under different environmental conditions. Based on the simulation results and quantitative analysis, the following key conclusions can be drawn:

1. The nested modeling approach effectively captures the rotational and translational characteristics of sea ice. Analysis of specific ice floes (such as sea ice 414) reveals that its rotational angle varies significantly over time under external forces, with distinct growth and decay patterns at different stages. The results indicate that sea ice rotation is influenced by local environment conditions, ice floe interactions, and external forces.

2. High-resolution numerical simulations provide refined insights into sea ice dynamics. Compared to traditional large-scale models, the nested model offers a more precise depiction of ice floe fracturing, rotation, and interactions. The simulations reveal that in densely packed regions, the movement of larger ice floes significantly affects the dynamics of surrounding smaller floes.

In conclusion, this study demonstrates that the nested modeling approach has high accuracy and applicability in simulating sea ice dynamics, effectively capturing its local evolution. The findings not only provide a more precise numerical tool for marine engineering and polar navigation but also lay a foundation for future improvements in sea ice dynamic models.

ACKNOWLEDGEMENTS

This work is supported by the National Key Technologies Research and Development Program (Grant No. 2022YFE0107000), National Natural Science Foundation of China (Grant No. 52171259), and High-tech ship research project of Ministry of Industry and Information Technology ([2021]342), and Science and Technology Commission of Shanghai Municipality Project (22DZ1204403，23YF1419900).

REFERENCES

Chassignet, E.P., H.E. Hurlburt, E.J. Metzger, O.M. Smedstad, J.A. Cummings, G.R. Halliwell, R. Bleck, R. Baraille, A.J. Wallcraft and C. Lozano, 2009. US GODAE Global

Ocean Prediction with the HYbrid Coordinate Ocean Model (HYCOM). *Oceanography*, vol 22, 64-75.

CICE Consortium, 2021. CICE Documentation. Available at: https://cice-consortium-590 cice.readthedocs.io/_/downloads/en/cice6.2.0/pdf/

Drusch, M., Del Bello, U., Carlier, S., Colin, O., Fernandez, V., Gascon, F., Hoersch, B., Isola, C., Laberinti, P., Martimort, P. and Meygret, A., 2012. Sentinel-2: ESA's optical high-resolution mission for GMES operational services. *Remote sensing of Environment*, 120, pp.25-36.

Howard, S.L., and Padman, L., 2021. *Arc2kmTM: Arctic 2 kilometer Tide Model, 2021.* Arctic Data Center.

Hunke, E.C. and Dukowicz, J.K., 1997. An elastic–viscous–plastic model for sea ice dynamics. *Journal of Physical Oceanography*, 27(9), pp.1849-1867.

Hunke, E., Allard, R., Blain, P., Blockley, E., Feltham, D., Fichefet, T., Garric, G., Grumbine, R., Lemieux, J.F., Rasmussen, T. and Ribergaard, M., 2020. Should sea-ice modeling tools designed for climate research be used for short-term forecasting?. *Current Climate Change Reports*, 6, pp.121-136.

Leppäranta, M., 2011. *The Drift of Sea Ice*. https://doi.org/10.1007/978-3-642-04683-4.

Liu Y, Wu H D., 2017. Sea ice dynamic. *Marine Forecasts*, 34(5): 99-110.

Lubbad, R., Løset, S., Lu, W., Tsarau, A. and van den Berg, M., 2018. An overview of the Oden Arctic Technology Research Cruise 2015 (OATRC2015) and numerical simulations performed with SAMS driven by data collected during the cruise. *Cold Regions Science and Technology*, 156, pp.1-22.

Ricker, R., Hendricks, S., Kaleschke, L., Tian-Kunze, X., King, J. and Haas, C., 2017. A weekly Arctic sea-ice thickness data record from merged CryoSat-2 and SMOS satellite data. *The Cryosphere*, 11(4), pp.1607-1623.

Solbrekke, I.M., Sorteberg, A. and Haakenstad, H., 2021. The 3 km Norwegian reanalysis (NORA3)–a validation of offshore wind resources in the North Sea and the Norwegian Sea.

Song L N, Shi W Q, Wang Z Z, et al., 2018. Real time monitoring sys tem for sea ice based on GPS and its application. *Journal of Glaciology and Geocryology*, 40(5): 960-965.

Tsarau, A., Lu, W., Lubbad, R., 2024a. Enhancing the Resolution of Large-Scale Sea-Ice Models Through Synthesising Satellite Imagery and Discrete-Element Modelling. *International Conference on Offshore Mechanics and Arctic Engineering*, Volume 6: Polar and Arctic Sciences and Technology; CFD, FSI, and AI.

Tsarau, A., Lu, W., Lubbad, R., Løset, S., Zhang, Y., 2024b. High-resolution regional sea-ice model based on the discrete element method with boundary conditions from a large-scale model for ice drift. *Annals of Glaciology*, 65:e25.

van den Berg, M., Lubbad, R. and Løset, S., 2018. An implicit time-stepping scheme and an improved contact model for ice-structure interaction simulations. *Cold Regions Science and Technology*, 155, pp.193-213.

Wang, S., Li, Y., Qiao, S., 2024. ALF-YOLO: Enhanced YOLOv8 based on multiscale attention feature fusion for ship detection. *Ocean Engineering*, 308: 118233.

Yu Y, Gu W, Xu Y J, et al., 2019. The in situ observation of modelled sea ice drift characteristics in the Bohai Sea. *Acta Oceanologica Sinica*, 38(3): 17-25.

Yuan S, Liu C, Liu X, et al., 2021 Research advances in remote sensing monitoring of sea ice in the Bohai sea. *Earth Science Informatics*, 14(4): 1729-1743.